Delay stabilization of rotating waves near fold bifurcation and application to all-optical control of a semiconductor laser

B. Fiedler[1], S. Yanchuk[2,3], V. Flunkert[4], P. Hövel[4], H.-J. Wünsche[5], and E. Schöll[4]

[1]*Institut für Mathematik I, FU Berlin,*

Arnimallee 2-6, D-14195 Berlin, Germany

[2]*Weierstraß Institut für Angewandte Analysis and Stochastik,*

Mohrenstr. 39, D-10117 Berlin, Germany

[3]*Humboldt Universität zu Berlin, Institut für Mathematik,*

Rudower Chaussee 25, D-12489 Berlin, Germany

[4]*Institut für Theoretische Physik, Technische Universität Berlin,*

Hardenbergstraße 36, D-10623 Berlin, Germany and

[5]*Humboldt Universität zu Berlin, Institut für Physik,*

Newtonstr. 15, D-12489 Berlin, Germany

Abstract

We consider the delayed feedback control method for stabilization of unstable rotating waves near a fold bifurcation. Theoretical analysis of a generic model and numerical bifurcation analysis of the rate-equations model demonstrate that such orbits can always be stabilized by a proper choice of control parameters. Our paper confirms the recently discovered invalidity of the so-called "odd-number-limitation" of delayed feedback control. Previous results have been restricted to the vicinity of a subcritical Hopf bifurcation. We now refute such a limitation for rotating waves near a fold bifurcation. We include an application to all-optical realization of the control in three-section semiconductor lasers.

I. INTRODUCTION

Control of complex irregular dynamics is one of the central issues in applied nonlinear science [1]. Starting with the work of Ott, Grebogi and Yorke [2], a variety of methods have been developed in order to stabilize unstable periodic orbits (UPOs) embedded in a chaotic attractor by employing tiny control forces. A particularly simple and efficient scheme is time-delayed feedback control as suggested by Pyragas [3]. In recent years the notion of *chaos control* has been extended to a much wider class of problems involving the stabilization of unstable periodic states in nonlinear dynamic systems, and has been applied to a vast range of problems in physics, chemistry, biology, medicine, and engineering. However, a deepened understanding of the control schemes and analytic insight into their potential limitations is still a challenging task.

Recently Fiedler *et al.* [4] have refuted an often invoked assertion, the so-called "odd-number limitation" of delayed feedback control. This purported limitation claims that a periodic orbit with an odd number of real Floquet multipliers greater than unity cannot be stabilized by the time-delayed feedback control in the form proposed by Pyragas [3]. The papers [4–6] show the possibility of stabilization of unstable periodic orbits, which are generated by a subcritical Hopf bifurcation. In our paper, we consider the case when the unstable periodic orbit is generated by a fold bifurcation of saddle-node type; see Eq. (1) below. We show that such orbits can be stabilized by delayed feedback control. We will restrict our analysis to the case when the periodic orbits have the special form of rotating waves. This case is particularly important for applications to optical systems and, in addition, allows detailed analytical treatment. One such system, a three-section semiconductor laser, will be considered in our paper. Numerical bifurcation analysis confirms that an all-optical delayed feedback control can successfully stabilize rotating waves close to a fold bifurcation in this system. All-optical control exploits the advantage of delayed feedback control, as well as simplicity and inherent high-speed operation. All-optical control of unstable steady states close to a supercritical Hopf bifurcation of the same system has been reported in Ref. [7].

The plan of our paper is as follows: Section II is devoted to the analytical treatment of a generic model for fold bifurcations of rotating waves. We derive necessary and sufficient conditions for successful control. In particular, we show that the stabilization can be achieved by delayed feedback with arbitrarily small control amplitude provided the phase

of the control is chosen appropriately. In Section III, we study a rate-equation model for three-section semiconductor lasers with all-optical delayed feedback. For suitably chosen parameter values, this model has a fold bifurcation. Numerical bifurcation analysis establishes successful control in the vicinity of this bifurcation.

II.   ANALYSIS OF FOLDS OF ROTATING WAVES

A.   Properties of the fold system without control

As a paradigm for fold bifurcation of rotating waves we consider planar systems of the form

$$\dot{z} = g(\lambda, |z|^2)z + ih(\lambda, |z|^2)z. \tag{1}$$

Here $z(t)$ is a scalar complex variable, g and h are real valued functions, and λ is a real parameter. Systems of the form (1) are S^1-equivariant, i.e., $e^{i\theta}z(t)$ is a solution whenever $z(t)$ is, for any fixed $e^{i\theta}$ in the unit circle S^1. In polar coordinates $z = re^{i\varphi}$ this manifests itself by absence of φ from the right hand sides of the resulting differential equations

$$\begin{aligned} \dot{r} &= g(\lambda, r^2)r, \\ \dot{\varphi} &= h(\lambda, r^2). \end{aligned} \tag{2}$$

In particular, all periodic solutions of Eq. (1) are indeed rotating waves, alias harmonic, of the form

$$z(t) = re^{i\omega t}$$

for suitable nonzero real constants r, ω. Specifically, this requires $\dot{r} = 0$, $\dot{\varphi} = \omega$:

$$\begin{aligned} 0 &= g(\lambda, r^2), \\ \omega &= h(\lambda, r^2). \end{aligned} \tag{3}$$

Fold bifurcations of rotating waves are generated by the nonlinearities

$$\begin{aligned} g(\lambda, r^2) &= (r^2 - 1)^2 - \lambda, \\ h(\lambda, r^2) &= \gamma(r^2 - 1) + \omega_0. \end{aligned} \tag{4}$$

Our choice of nonlinearities is generic in the sense that $g(\lambda, r^2)$ is the normal form for a nondegenerate fold bifurcation [8] at $r^2 = 1$ and $\lambda = 0$. See Fig. 1 for the resulting bifurcation diagram. We fix coefficients $\gamma, \omega_0 > 0$.
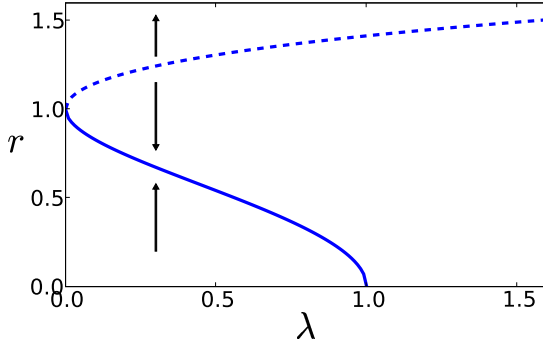
Figure 1: Bifurcation diagram of rotating waves (solid line: stable; dashed line: unstable) of Eqs. (1) and (4). Arrows indicate (in-)stability according to Eq. (2).

Using Eqs. (3) and (4), the amplitude r and frequency ω of the rotating waves then satisfy

$$r^2 = 1 \pm \sqrt{\lambda}, \quad \omega = \omega_0 + \gamma(r^2 - 1) = \omega_0 \pm \gamma\sqrt{\lambda}. \tag{5}$$

The signs $\pm$ correspond to different branches in Fig. 1, $+$ unstable and $-$ stable.

B.   Fold system with delayed feedback control

Our goal is to investigate delay stabilization of the fold system (1) by the delayed feedback term

$$\dot{z} = f(\lambda, |z|^2)z + b_0 e^{i\beta} \left[z(t - \tau) - z(t)\right], \tag{6}$$

with real positive control amplitude b_0, delay τ, and real control phase β. Here we have used the abbreviation $f = g + ih$. The Pyragas choice requires the delay τ to be an integer multiple k of the minimum period T of the periodic solution to be stabilized:

$$\tau = kT. \tag{7}$$

This choice guarantees that periodic orbits of the original system (1) with period T are reproduced exactly and noninvasively by the control system (6). The minimum period T of a rotating wave $z = re^{i\omega t}$ is given explicitly by $T = 2\pi/\omega$. Using Eqs. (5), Eq. (7) becomes

$$\tau = \frac{2\pi k}{\omega_0 \pm \gamma\sqrt{\lambda}}, \tag{8}$$

or, equivalently,

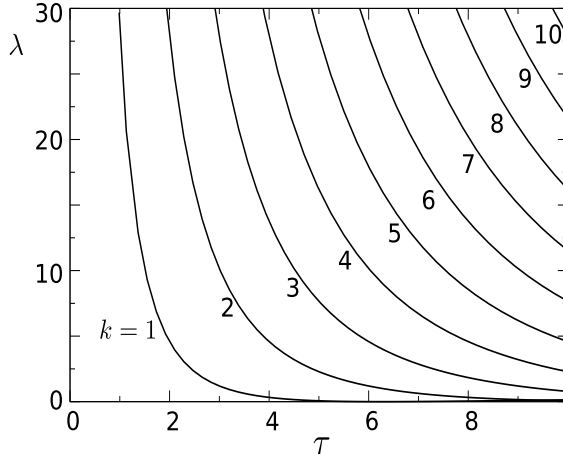$$\lambda = \lambda(\tau) = \left(\frac{2\pi k - \omega_0 \tau}{\gamma \tau}\right)^2. \tag{9}$$

4

Figure 2: The Pyragas curves $\lambda = \lambda(\tau)$, corresponding to the unstable branch in Fig. 1, in the parameter plane (τ, λ); see Eq. (9). Parameters: $\gamma = \omega_0 = 1$.

In the following we select only the branch of $\lambda(\tau)$ corresponding to the τ-value with the $+$ sign, which is associated with the unstable orbit. Condition (9) then determines the k-th *Pyragas curve* in parameter space (τ, λ) where the delayed feedback is noninvasive, indeed. The fold parameter $\lambda = 0$ corresponds to $\tau = 2\pi k/\omega_0$, along the k-th Pyragas curve. See Fig. 2 for the Pyragas curves in the parameter plane (τ, λ).

For the delay stabilization system (6) we now consider τ as the relevant bifurcation parameter. We restrict our study of Eq. (6) to $\lambda = \lambda(\tau)$ given by the Pyragas curve (9), because $\tau = kT$ is the primary condition for noninvasive delayed feedback control.

We begin with the trivial case $b_0 = 0$ of vanishing control, somewhat pedantically; see Section II A. For each $\lambda = \lambda(\tau)$, we encounter two rotating waves given by

$$r^2 = 1 \pm \frac{2\pi k - \omega_0 \tau}{\gamma \tau}, \quad \omega = \omega_0 \pm \left(\frac{2\pi k - \omega_0 \tau}{\tau} \right). \tag{10}$$

The two resulting branches form a transcritical bifurcation at $\tau = 2\pi k/\omega_0$. At this stage, the transcriticality looks like an artefact, spuriously caused by our choice of the Pyragas curve $\lambda = \lambda(\tau)$. Note, however, that only one of the two crossing branches features minimum period T such that the Pyragas condition $\tau = kT$ holds. This happens along the branch

$$r^2 = 1 + \frac{2\pi k - \omega_0 \tau}{\gamma \tau}, \quad \omega = 2\pi k/\tau,$$

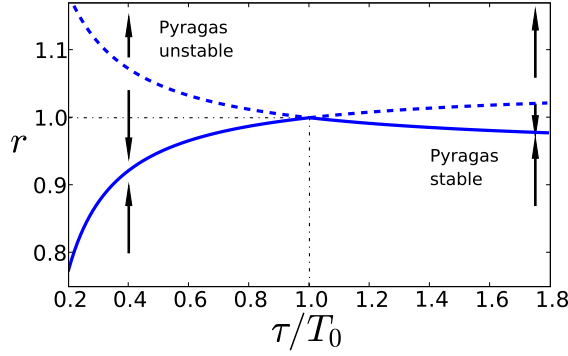see Fig. 3. We call this branch, which corresponds to '+' in Eq. (10) the *Pyragas branch*.

5

Figure 3: Bifurcation diagram of rotating waves of Eq. (6) at vanishing control amplitude $b_0 = 0$. Parameters: $T_0 = 2\pi/\omega_0$, $\omega_0 = 1$, $\gamma = 10$.

The other branch has minimum period T with

$$kT = \frac{\pi k}{\omega_0 \tau - \pi k}\tau \neq \tau,$$

except at the crossing point $\omega_0 \tau = 2\pi k$. The minus-branch therefore violates the Pyragas condition for non-invasive control, even though it has admittedly been generated from the same fold bifurcation.

Our strategy for Pyragas control of the unstable part of the Pyragas branch is now simple. For a nonzero control amplitude b_0, the Pyragas branch persists without change, due to the noninvasive property $\tau = kT$ along the Pyragas curve $\lambda = \lambda(\tau)$. The minus-branch, however, will be perturbed slightly for small $b_0 \neq 0$. If the resulting perturbed transcritical bifurcation

$$\tau = \tau_c \tag{11}$$

moves to the left, i.e., below $2\pi k/\omega_0$, then the stability region of the Pyragas branch has invaded the unstable region of the fold bifurcation. Again this refutes the notorious odd number limitation of Pyragas control, see Fiedler *et al.* [4] and references therein.

Let $\tau = \tau_c$ denote the transcritical bifurcation point on the Pyragas curve $\lambda = \lambda(\tau)$; see Eq. (9). Let $z(t) = r_c e^{i\omega_c t}$ denote the corresponding rotating wave, and abbreviate $\varepsilon \equiv r_c^2 - 1$. In Appendix A, we obtain conditions for the transcritical bifurcation in Eq. (6). As a result, the following relations between the control amplitude b_c at the bifurcation and ε, τ_c are shown:

$$b_c = -\varepsilon \frac{\omega_0 + \gamma\varepsilon}{k\pi(\gamma \sin \beta + 2\varepsilon \cos \beta)} \tag{12}$$

6

and

$$b_c = -\frac{2\pi k - \omega_0 \tau_c}{\tau_c \left(\frac{1}{2}\gamma^2 \tau_c \sin\beta + (2\pi k - \omega_0 \tau_c)\cos\beta\right)}. \tag{13}$$

As follows from Eqs. (12) and (13), for small ε, alias for τ_c near $2k\pi/\omega_0$, *the optimal control angle is $\beta = -\pi/2$ in the limit* $\varepsilon \to 0$, and for fixed $k, \omega_0, \gamma, \varepsilon$ this control phase β allows for stabilization with the smallest amplitude $|b_c|$. For $\beta = -\pi/2$ the relations Eqs. (12) and (13) simplify to

$$b_c = \frac{\varepsilon}{k\pi}\left(\frac{\omega_0}{\gamma} + \varepsilon\right) \tag{14}$$

and

$$b_c = \frac{2}{(\gamma\tau_c)^2}(2k\pi - \omega_0\tau_c), \tag{15}$$

respectively. For small $b_0 > 0$ we also have the expansions

$$\varepsilon = -\left(k\pi\frac{\gamma}{\omega_0}\sin\beta\right)b_0 + \cdots \tag{16}$$

and

$$\tau_c = \frac{2\pi k}{\omega_0} + \left(\frac{1}{2\omega_0}\left(\frac{2k\pi\gamma}{\omega_0}\right)^2\sin\beta\right)b_0 + \cdots. \tag{17}$$

for the location of the transcritical bifurcation. In particular we see that *odd number delay stabilization can be achieved by arbitrary small control amplitudes b_0 near the fold, for $\gamma > 0$ and $\sin\beta < 0$.* Note that the stability region of the Pyragas curve increases if $\varepsilon = r_c^2 - 1 > 0$; see Fig. 1. *For vanishing phase angle of the control, $\beta = 0$, in contrast, delay stabilization cannot be achieved by arbitrarily small control amplitudes b_0, near the fold in our system (6).*

Even far from the fold at $\lambda = 0$, $\tau = 2k\pi/\omega_0$ the above formulas (12) – (15) hold and indicate a transcritical bifurcation from the (global) Pyragas branch of rotating waves of Eq. (6), along the Pyragas curve $\lambda = \lambda(\tau)$. This follows by analytic continuation. Delay stabilization, however, may fail long before $\tau = \tau_c$ is reached. In fact, nonzero purely imaginary Floquet exponents may arise, which destabilize the Pyragas branch long before $\tau = \tau_c$ is reached. This interesting point remains open.

A more global picture of the orbits involved in the transcritical bifurcation may be obtained by numerical analysis. Rewriting Eq. (6) in polar coordinates $z = re^{i\varphi}$ yields

$$\begin{aligned}\dot{r} &= [(r^2-1)^2 - \lambda]r \\ &+ b_0[\cos(\beta + \varphi(t-\tau) - \varphi)\,r(t-\tau) - r\cos\beta]\end{aligned} \tag{18}$$

$$\dot{\varphi} = \gamma(r^2 - 1) + \omega_0 \tag{19}$$
$$+ b_0[\sin(\beta + \varphi(t - \tau) - \varphi)\, r(t - \tau)/r - \sin\beta].$$

To find all rotating wave solutions we make the ansatz $r = \text{const}$ and $\dot{\varphi} = \omega = \text{const}$ and obtain

$$0 = (r^2 - 1)^2 - \lambda + b_0[\cos(\beta - \omega\tau) - \cos\beta]$$
$$\omega = \gamma(r^2 - 1) + \omega_0 + b_0[\sin(\beta - \omega\tau) - \sin\beta].$$

Eliminating r we find a transcendental equation for ω

$$0 = -\gamma^2\lambda + \gamma^2 b_0[\cos(\beta - \omega\tau) - \cos\beta]$$
$$+ (\omega - \omega_0 - b_0[\sin(\beta - \omega\tau) - \sin\beta])^2.$$

One can now solve this equation numerically for ω and insert the result into

$$r = \left(\frac{\omega - \omega_0}{\gamma} - \frac{b_0}{\gamma}[\sin(\beta - \omega\tau) - \sin\beta] + 1\right)^{\frac{1}{2}}$$

to obtain the allowed radii (discarding imaginary radii).

The orbit which stabilizes the Pyragas branch in the transcritical bifurcation may be the minus-branch or another delay induced orbit which is born in a fold bifurcation, depending on the parameters. Figure 4 displays the different scenarios and the crossover in dependence on the control amplitude b_0. The value of γ is chosen as $\gamma = 9$, 10.5, 10.6, and 13 in panels (a), (b), (c), and (d), respectively. It can be seen that the Pyragas orbit is stabilized by a transcritical bifurcation T_1. As the value of γ increases, a pair of a stable and an unstable orbit generated by a fold bifurcation F_1 approaches the minus-branch (see Fig. 4(a)). On this branch, fold bifurcations (F_2 and F_3) occur as shown in Fig. 4(b). At $\gamma = 10.6$, the fold points of F_1 and F_2 touch in a transcritical bifurcation T_2 and annihilate (see Figs. 4(c) and (d)). Thus, for further increase of γ, one is left with the stable minus-branch and the unstable orbit, which was generated at the fold bifurcation F_3. In all panels the radius of the Pyragas orbit is not changed by the control. The radius of the minus-branch, however, is altered because the delay time does not match orbit period.

Figure 5 shows the region in the (β, b_0) plane where the Pyragas orbit is stable, for a set of parameters. The grayscale (color code) shows only negative values of the largest real part of the Floquet exponents. One can see that the orbit is most stable for feedback phases
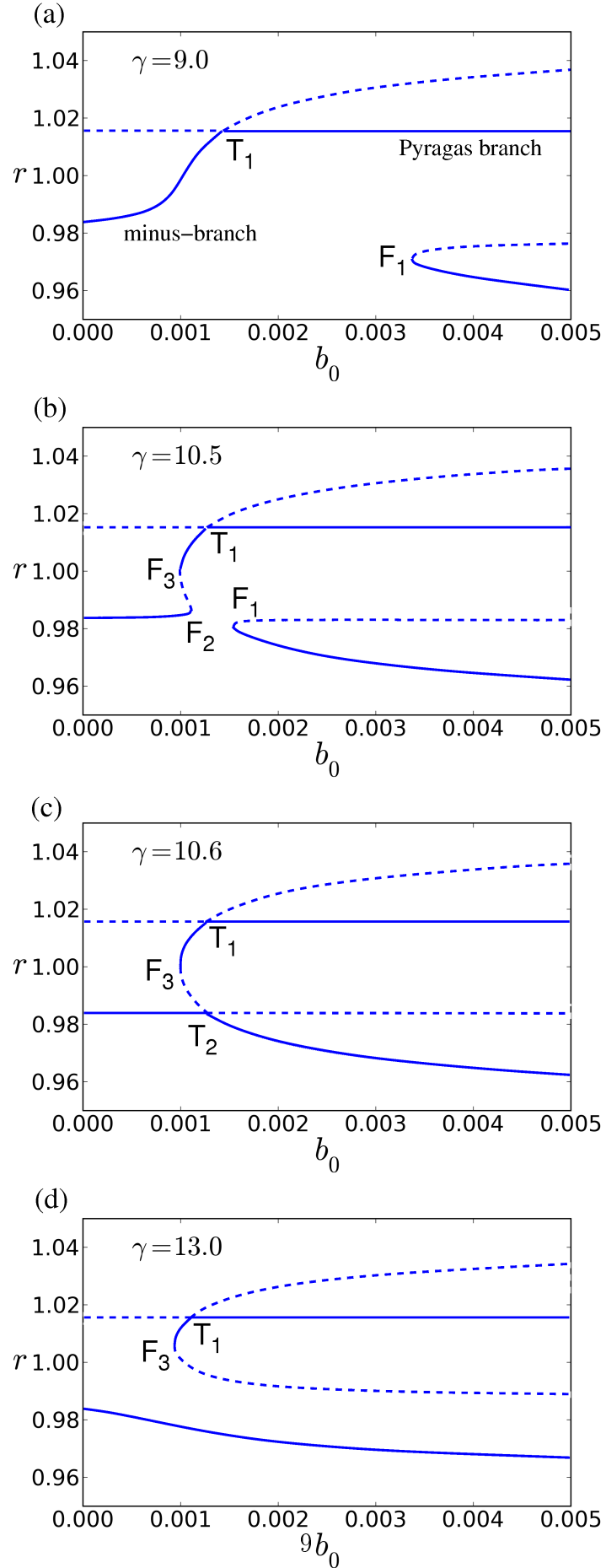
Figure 4: Radii of stable (solid) and unstable (dashed) rotating wave solutions in dependence on b_0 for different γ. Parameters: $\omega_0 = 1$, $\lambda = 0.001$, $\beta = -\pi/2$.
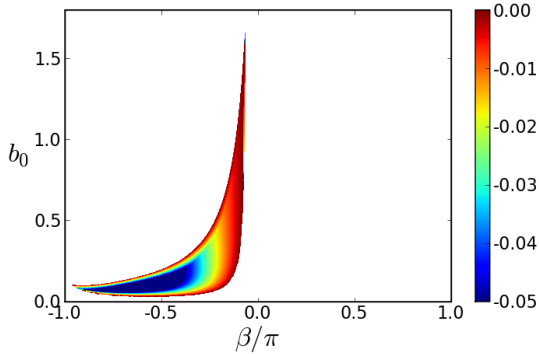
Figure 5: (Color online) Domain of stability of the Pyragas orbit. The grayscale (color code) shows only negative values of the largest real part of the Floquet exponents. Parameters: $\omega_0 = 1$, $\lambda = 0.0001$, $\gamma = 0.1$. Cf. also Fig. 11.

$\beta \approx -\pi/2$ which agrees with the previous analytic results for small λ. The picture was obtained by linear stability analysis of Eqs. (18) and (19) and numerical solution of the transcendental eigenvalue problem for the Floquet exponents (see Appendix B).

III. APPLICATION TO ALL-OPTICAL CONTROL OF SEMICONDUCTOR LASERS

Lasers in stationary states emit rotating waves. A first step towards various instabilities is often the destruction of these states or the creation of additional ones in fold bifurcations. This happens generically when a laser is coupled to other lasers or to external cavities [9]. In what follows, we investigate to what extent the results of Section II can be transfered to lasers in such situations. In particular, we consider an integrated tandem laser (ITL), which is integrating two single-mode lasers coupled by a passive waveguide section on a monolithic semiconductor chip (cf. Fig. 6). Devices of this type are applied in ultrafast optical communication [10, 11]. Depending on pump currents they exhibit different types of bifurcations and dynamics at tens of GHz, and THz are within reach [12, 13]. Control on those ultra-short picosecond timescales can be performed only in the optical domain, which profits from the ultimately high speed of light. Two schemes have been proposed: optical feedback either from a Michelson interferometer [14] or from a Fabry-Perót interferometer [15]. Experimental all-optical time delayed feedback control has been developed only re-

10

cently, exploiting optical feedback from a Fabry-Perót interferometer to stabilize unstable steady states of an ITL close to a Hopf bifurcation [7]. In the present work we consider the Michelson configuration [14], which is the optical version of the Pyragas method. The corresponding scheme is sketched in Fig. 6.
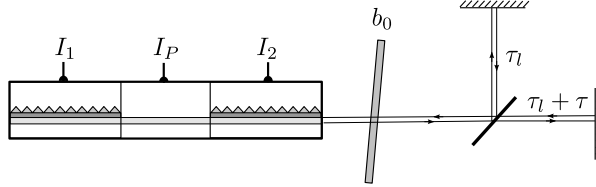

Figure 6: Schematic diagram for all-optical delayed feedback control. The emission from one facet of an integrated tandem laser is injected into a Michelson interferometer. Two reflected waves return from there with different delays τ_l and $\tau_l + \tau$. Their superposition is reinjected into the device and serves as control force. The amplitude b_0 of the control is adjusted by a neutral density filter. The control phase β rotates by 2π when changing the pathway between laser and interferometer by one wavelength.

A.   System without control

In order to describe the dynamics, we use the coupled rate-equations model for ITL lasers in dimensionless form [16]

$$\dot{E}_1 = i\delta E_1 + (1 + i\alpha)N_1 E_1 + \eta e^{-i\varphi} E_2, \tag{20}$$

$$\dot{N}_1 = \varepsilon \left[J - N_1 - (1 + 2N_1)\left|E_1\right|^2 \right], \tag{21}$$

$$\dot{E}_2 = (1 + i\alpha)N_2 E_2 + \eta e^{-i\varphi} E_1 + E_b(t), \tag{22}$$

$$\dot{N}_2 = \varepsilon \left[J - N_2 - (1 + 2N_2)\left|E_2\right|^2 \right], \tag{23}$$

extended by the control term $E_b(t)$, which is disregarded for the moment and will be specified later (in Eq. (25)). The complex amplitudes $E_{1,2}$ and the real quantities $N_{1,2}$ represent the optical fields and the carrier densities in the two single-mode distributed feedback (DFB) lasers, respectively; δ accounts for the frequency detuning between them; J stands for pumping currents; η and φ characterize the coupling rate and the optical phase shift, respectively, between the two DFB sections; α denotes the linewidth-enhancement factor characterizing

11

the amplitude-phase coupling typical for semiconductor lasers; $\varepsilon = \tau_p/\tau_n$ is the ratio between photon (τ_p) and carrier (τ_n) lifetimes, and τ_p serves as unit of time. It is important to know that $E_{1,2}(t)$ represent slowly varying amplitudes. The full temporal variation of the optical fields is

$$\mathcal{E}_{1,2}(t) = E_{1,2}(t)e^{i\omega_0 t} \tag{24}$$

with the optical reference frequency ω_0 playing the role of the corresponding quantity ω_0 in Section II. In the present formulation, ω_0 is the optical frequency of laser 2 in its unperturbed ($\eta = E_b = 0$) stationary state $N_2 = 0$, $E_2 =$const. At communication wavelengths around $\lambda = 1.55\ \mu$m, we have $\omega_0 \approx 10^{15}$s^{-1}. The corresponding dimensionless value is 50000 when assuming $\tau_p = 5$ ps. The dynamics of $E(t)$ and $N(t)$ takes place on timescales which are by more than 3 orders of magnitude slower.

System (20) – (23) without control, i.e., $E_b = 0$, was considered in detail in Ref. [16]. Rotational symmetry manifests itself by the invariance with respect to the transformation $(E_1, E_2) \mapsto (e^{i\theta}E_1, e^{i\theta}E_2)$ for any $e^{i\theta}$ in the unit circle S^1. This causes periodic solutions in the form of rotating waves $(E_1, N_1, E_2, N_2) = (a_1e^{i\omega t}, n_1, a_2e^{i\omega t}, n_2)$ with real constants ω, n_1, n_2 and complex constants a_1 and a_2. When varying the phase φ of the internal coupling between the two DFB lasers, the rotating waves lose stability either in a Hopf bifurcation or in a fold bifurcation as shown in a typical bifurcation diagram presented in Fig. 7. The Hopf bifurcation gives rise to periodically modulated waves, called self-pulsations, which will not be considered furthermore. In the present context, we consider the problem of stabilization of unstable rotating waves close to the fold F. The frequencies ω of rotating waves near F are drawn in panel (b). They increase when moving up through F in concordance with the scenario $\gamma > 0$ considered in Section II. Thus, we can expect that the stabilization of the unstable branch by Pyragas-type feedback should be possible.

B. The optical control force

Under which conditions does optical feedback from a Michelson interferometer give rise to a Pyragas-type control term $E_b(t)$? Generally, E_b is proportional to the slowly varying amplitude of the light fed back from the interferometer, which in turn is the sum of two
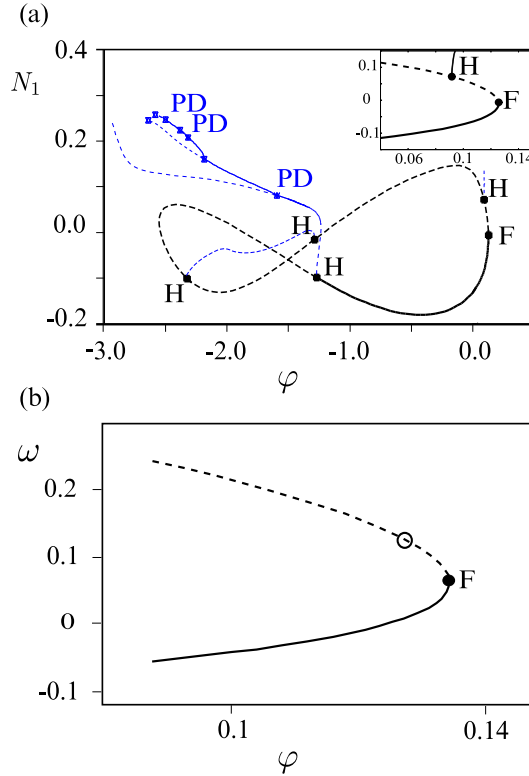
Figure 7: (Color online) (a): Bifurcation diagram for the system (20) – (23) without control, i.e., $b_0 = 0$. Inset: a zoom close to the fold bifurcation F. Thick lines: rotating waves; thin lines: modulated waves (self-pulsations). Stable and unstable parts of the diagram are shown by solid lines and dashed lines respectively. H: Hopf bifurcation; PD: periodic doubling of self-pulsations. (b): frequencies of rotating waves close to the fold bifurcation of panel (a). Open circle: exemplary target state for stabilization. Other parameters are $\varepsilon = 0.03$, $J = 1$, $\eta = 0.2$, $\delta = 0.3$, $\alpha = 2$.

partial waves, each one reflected from a different mirror. Accordingly,

$$E_b(t) = b_0 e^{i\beta} \left[e^{i\psi} E_2(t - \tau_l - \tau) - E_2(t - \tau_l) \right]. \tag{25}$$

τ_l and $\tau_l + \tau$ are the travel times of light on the two pathways. τ corresponds to the control delay time of Eq. (6) and τ_l is an additional latency, which unavoidably occurs in real systems. The two optical phase shifts $\beta = -(\omega_0 \tau_l + \pi)$ and $\psi = -(\omega_0 \tau + \pi)$ are associated with the respective delays. They are the impact of the fast optical phase rotation (24) on the slow amplitudes of delayed light. The π is added in both cases to obtain consistency with the choice of signs in Section II. Further possible phase shifts, e.g., from reflections at mirrors may also be incorporated this way. Both phases are tunable by subwavelength

13

changes of the respective optical pathways which have no effect on the slow amplitudes. Thus, they are regarded as independent parameters. The feedback amplitude b_0 contains all attenuations on the respective round trips. Note that equal attenuation on both pathways is assumed, otherwise destructive interference remains incomplete and noninvasiveness is not achievable. Noninvasiveness also requires proper adjustment of phase ψ. Indeed, when the target state is a rotating wave $E_2(t) = a_2 e^{i\omega t}$, the control term vanishes for $e^{i(\psi - \omega \tau)} = 1$. This is the well-known condition for destructive interference: nothing is reflected if the two returning partial waves have opposite amplitudes. Control phase β and amplitude b_0 are free parameters playing the same role as the corresponding quantities in Section II.

C.   Stabilization of rotating waves

Now we study stabilization of rotating waves on the unstable branch close to the fold bifurcation in Fig. 7. We fix the delays of the control term as $\tau_l = 8$ and $\tau = 12$, corresponding to about 40 ps and 60 ps, respectively, which are accessible in experiment [7]. These parameters are not critical, other values of the same order yield similar results.

Exemplarily, we address the unstable state $\omega = 0.1109$ at $\varphi = 0.1267$ (open circle in Fig. 7(b)), which without control indeed has a single positive Floquet exponent [20] (Fig. 8(a)). With control ($b_0 > 0$), this target state itself does not get light back and keeps unchanged by setting $\psi = \omega \tau = 1.3308$. Only deviations from it cause a nonvanishing feedback, which in fact modifies its stability. These effects and the resulting bifurcations have been calculated by applying the software package DDE-BIFTOOL [17] to the delay-differential system (20) – (23). Now the leading Floquet exponents change with b_0 is plotted in Fig. 8(b) for $\beta = 0$. With increasing b_0, the unstable real Floquet exponent decreases and becomes negative in point T. This stabilization is due to a transcritical bifurcation T, as predicted in Section II. In terms of the Floquet multipliers this indicates that an unstable multiplier crosses the unit circle at 1. With further increase of the control parameter b_0, first, two branches of eigenvalues with negative real parts coalesce and then a destabilization takes place, when the two complex conjugate eigenvalues become unstable, i.e., a Hopf bifurcation to self-pulsating solutions occurs in point H in Fig. 8(b). The zero line in Fig. 8(b) corresponds to the trivial Floquet exponent, which occurs due to the symmetry and does not influence the stability.

A two-parameter bifurcation diagram of the same rotating wave in the plane (β, b_0) is
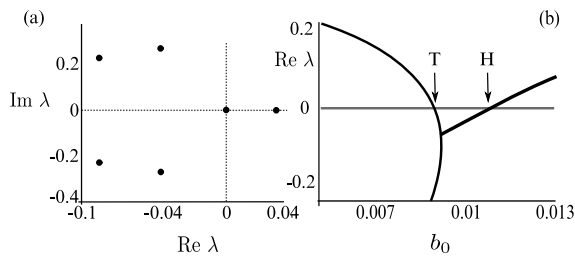
Figure 8: (a) Floquet exponents of the uncontrolled target state. (b) Real part of leading Floquet exponents of the target state as a function of b_0 for $\beta = 0$. T denotes transcritical and H Hopf bifurcations, respectively. Parameters are $\varepsilon = 0.03$, $J = 1$, $\eta = 0.2$ $\delta = 0.3$, $\alpha = 2$, $\omega = 0.1109$, $\varphi = 0.1267$, $\tau_l = 8$, $\tau = 12$ and $\psi = \omega\tau$.

shown in Fig. 9. The stability region is bounded by the Hopf and transcritical bifurcations mentioned before. The role of these bifurcations is as predicted by the generic model in Section II and also the shape is similar to that of Fig. 5. It is interesting to compare this bifurcation diagram to other known cases of all-optical control. A simple single-mode laser exposed to noninvasive control of type (25) changes stability similarly by transcritical and Hopf bifurcations [18] – only the laser is destabilized but not stabilized. In case of rotating waves beyond a Hopf bifurcation in an ITL laser, the domains of control are also bounded by Hopf and transcritical bifurcations but with different ordering: inverse Hopf defines the lower bound whereas the upper bound is partly transcritical [7, 19]. Quantitatively, the vertical extension of the present control domain near a fold bifurcation is, however, small compared to the latter case. Thus, a possible experimental stabilization near folds will probably require a more precise adjustment of control amplitude b_0 compared to Refs. [7, 19].

To investigate the influence of the control on the environment of the target state, we recalculated the bifurcation diagram of Fig. 7(b) with control parameters on the vertical line 2 in Fig. 9. The resulting branches of rotating waves are compared to those of the uncontrolled device in Fig. 10. Panel (a) exemplifies the particular case $b_0 = 0.005$. Apart from the target state (open circle), which keeps unchanged on purpose, the feedback is invasive and changes the laser state. Due to the smallness of b_0, the modifications are minor (note the small zoom compared to full bifurcation diagram Fig. 9(a). The fold bifurcation is preserved and shifted slightly above the target state. As a consequence, the target is now
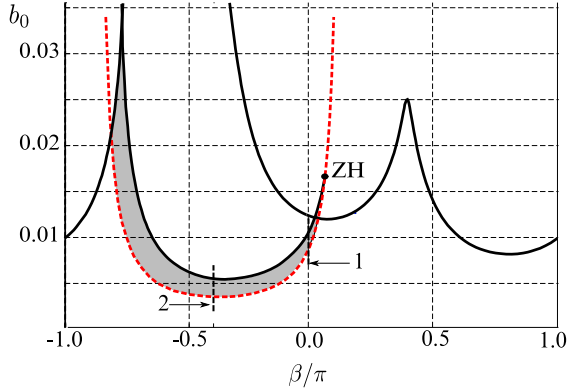
15

Figure 9: (Color online) Two-dimensional bifurcation diagram of the target state with respect to the control parameters b_0 and β. Black solid: Hopf bifurcation. Above this line the laser emits self pulsations. Red dashed: transcritical bifurcation. Below this line, the target state is unstable. Gray area denotes the stability region. ZH is the zero-Hopf bifurcation of codimension two. Line 1 corresponds to the parameter path along which the eigenvalues are computed in Fig. 8(b). Line 2 corresponds to the parameter changes in Fig. 10. Other parameters as in Fig. 8.

on the stable branch. The stabilization transition happens when the fold bifurcation crosses the unstable branch of the uncontrolled system exactly in the target state. The target is the upper of the two states with $\varphi = 0.1267$; it is unstable for smaller b_0 (curve 1) and stable for larger b_0 (curve 3). Both states cross in a transcritical bifurcation (inset), in agreement with the results of Section II.

IV. CONCLUSIONS

We have shown that, contrary to common belief, unstable periodic states with an odd number of real Floquet multipliers greater than unity, here created by a fold bifurcation, can indeed be stabilized by time delayed feedback control. As a promising all-optical realization we propose an integrated semiconductor tandem laser combined with a Michelson interferometer.

Our analysis is complementary to the previous publications on this topic [4–6], which have been devoted to the stabilization of unstable periodic orbits close to a subcritical Hopf bifurcation. The approaches which have been used in the above papers are specifically based on the normal form at the subcritical Hopf bifurcation and can not be simply transferred
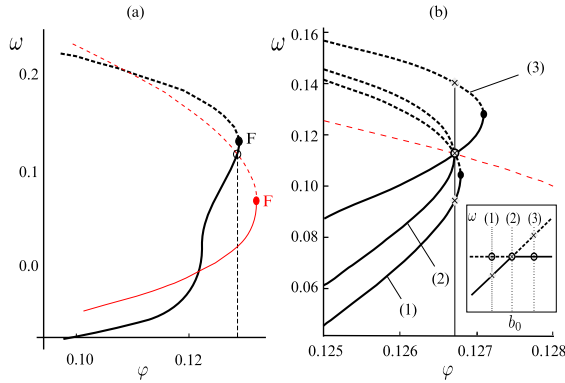
Figure 10: (Color online) Branches of stable (solid) and unstable (dashed) rotating waves without control (thin, red) and with control (black, thick). F: fold bifurcation. Vertical line: $\varphi = 0.1267$ of the chosen target state. Open circle: target state. (a): $b_0 = 0.005$. (b): (1) $b_0 = 0.0030$ below, (2) $b_0 = 0.0035$ at, (3) $b_0 = 0.0050$ above the control threshold. Inset: relation to the transcritical bifurcation. Parameters as in Fig. 9 and $\beta = -0.408\pi$, $\psi = 1.3308$.

to the fold case. The common point in both scenarios of stabilization is the appearance of a transcritical bifurcation resulting from the two basic assumptions: vanishing control term for the Pyragas orbit, and the existence of one unstable real positive Floquet multiplier.

Note that one can perturb the equations (6), or (20) − (23), such that the S^1 symmetry is broken. In this case the stable (unstable) rotating waves will be perturbed into stable (unstable) periodic solutions, respectively, which will no longer have the form of rotating waves. Thus, by rigorous perturbative arguments, our paper refutes the odd-number limitation also for periodic solutions which are not rotating waves. On the other hand, in non-autonomous systems the odd-number limitation may still hold [5].

Acknowledgments

We gratefully acknowledge the support of DFG in the framework of Sfb555.

Appendix A

In this Appendix, we derive conditions (12) and (13) at which the transcritical bifurcation in system (6) occurs. To derive Eq. (12) we could proceed by brute force: linearize the control system (6) along the Pyragas branch, in polar coordinates, derive the characteristic

17

equation in a co-rotating coordinate frame, eliminate the trivial zero characteristic root, and determine $\tau = \tau_c$, $r = r_c$, and $b_0 = b_c$ such that a nontrivial zero characteristic root remains. Instead, we will proceed locally in a two-dimensional center manifold of the fold, following the arguments in Just *et al.* [5], as given in Appendix B below. Any periodic solution in the center manifold of Eq. (6) is a rotating wave $z(t) = re^{i\omega t}$.

Hence, let us compute the rotating waves of the system (6), globally. Substituting $z(t) = re^{i\omega t}$ into Eq. (6) and decomposing into real and imaginary parts, we obtain

$$0 = g(\lambda, r^2) + 2b_0 \sin \frac{\omega\tau}{2} \sin \left(\beta - \frac{\omega\tau}{2}\right), \tag{26}$$

$$\omega = h(\lambda, r^2) - 2b_0 \sin \frac{\omega\tau}{2} \cos \left(\beta - \frac{\omega\tau}{2}\right). \tag{27}$$

With $\varepsilon = r^2 - 1$ and our choices (4) for g and h, these equations become

$$0 = \varepsilon^2 - \lambda(\tau) + 2b_0 \sin \frac{\omega\tau}{2} \sin \left(\beta - \frac{\omega\tau}{2}\right), \tag{28}$$

$$\omega = \gamma\varepsilon + \omega_0 - 2b_0 \sin \frac{\omega\tau}{2} \cos \left(\beta - \frac{\omega\tau}{2}\right). \tag{29}$$

For small enough b_0, we can solve Eq. (29) for $\omega = \omega(\varepsilon)$ and insert into Eq. (28):

$$0 = G(\tau, \varepsilon). \tag{30}$$

Here $G(\tau, \varepsilon)$ abbreviates the right hand side of Eq. (28) with $\omega = \omega(\varepsilon)$ substituted for ω. The condition for a transcritical bifurcation in the system with control then reads

$$0 = \frac{\partial}{\partial\varepsilon} G(\tau_c, \varepsilon) \tag{31}$$

in addition to Eq. (30). It simplifies matters significantly that this calculation has to be performed along the Pyragas branch only, where $\omega\tau = 2\pi\tau/T = 2\pi k$; see Eq. (7). Therefore Eq. (31) becomes

$$\begin{aligned} 0 &= \frac{\partial}{\partial\varepsilon} G(\tau_c, \varepsilon) \\ &= 2\varepsilon + b_0 \tau_c \cos k\pi \sin (\beta - k\pi) \omega'(\varepsilon) \\ &= 2\varepsilon + b_0 \tau_c \omega'(\varepsilon) \sin \beta. \end{aligned} \tag{32}$$

To obtain the derivative ω' of ω with respect to ε we have to differentiate Eq. (29) implicitly, at $\omega\tau = 2k\pi$

$$\omega' = \gamma - b_0 \tau \omega' \cos \beta.$$

18

Solving for ω', for small b_0, yields

$$\omega' = \frac{\gamma}{1 + b_0 \tau \cos\beta} = \frac{\gamma}{1 + b_0 \frac{2k\pi}{\omega_0 + \gamma\varepsilon} \cos\beta}. \tag{33}$$

Here we have used $\omega\tau = 2k\pi$ and $\omega = \omega_0 + \gamma\varepsilon$. Plugging Eq. (33) into Eq. (32), the control amplitude b_0 enters linearly, and we obtain

$$\begin{aligned} 0 &= \varepsilon\left(\omega_0 + \gamma\varepsilon\right)\left(1 + b_0\frac{2k\pi}{\omega_0 + \gamma\varepsilon}\cos\beta\right) + b_0 k\pi\gamma\sin\beta \\ &= \varepsilon\left(\omega_0 + \gamma\varepsilon + b_0 2k\pi\cos\beta\right) + b_0 k\pi\gamma\sin\beta. \end{aligned} \tag{34}$$

Solving for b_0, we obtain the required expression (12) for the value of the control amplitude, at which the transcritical bifurcation occurs.

The equivalent condition (13) follows from Eq. (12) by straightforward substitution of Eq. (8) and $-\sqrt{\lambda} = r^2 - 1 = \varepsilon$.

Appendix B

In this Appendix we perform a linear stability analysis of the Pyragas orbit. Linearizing Eqs. (18) and (19) around the Pyragas orbit according to $z(t) = (r + \delta r)\exp(i\omega t + i\delta\varphi)$, we find

$$\begin{aligned} \frac{d}{dt}\begin{pmatrix} \delta r(t) \\ \delta\varphi(t) \end{pmatrix} &= \begin{bmatrix} \partial_r g\, r + g - b_0\cos\beta & rb_0\sin(\beta - \omega\tau) \\ \partial_r h - b_0\sin(\beta - \omega\tau)\frac{1}{r} & -b_0\cos(\beta - \omega\tau) \end{bmatrix}\begin{pmatrix} \delta r(t) \\ \delta\varphi(t) \end{pmatrix} \\ &+ \begin{bmatrix} b_0\cos(\beta - \omega\tau) & -rb_0\sin(\beta - \omega\tau) \\ b_0\sin(\beta - \omega\tau)/r & b_0\cos(\beta - \omega\tau) \end{bmatrix}\begin{pmatrix} \delta r(t - \tau) \\ \delta\varphi(t - \tau) \end{pmatrix}. \end{aligned}$$

The delay time τ matches the period of the Pyragas orbit and we thus have

$$\omega\tau = 2\pi k.$$

Using the exponential ansatz $(\delta r(t), \delta\varphi(t)) \propto \exp\Lambda t$ gives a transcendental equation for the Floquet exponents Λ:

$$\det\begin{bmatrix} 4(r^2 - 1)r^2 + (r^2 - 1)^2 - \lambda - \Lambda - b_0\cos\beta\left(1 - e^{-\Lambda\tau}\right) & rb_0\sin\beta\left(1 - e^{-\Lambda\tau}\right) \\ 2\gamma r - (b_0/r)\sin\beta\left(1 - e^{-\Lambda\tau}\right) & -\Lambda - b_0\cos\beta\left(1 - e^{-\Lambda\tau}\right) \end{bmatrix} = 0. \tag{35}$$
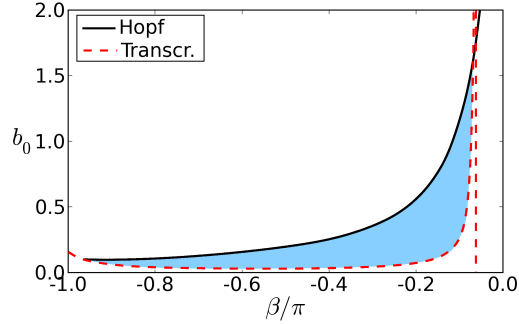
Figure 11: (Color online) Plot of transcritical (dashed) and Hopf bifurcation line (solid) and domain of stability (shaded region) in the (β, b_0) plane. Parameters as in Fig. 5

This equation was numerically solved to obtain Fig. 5.

One can find the Hopf bifurcation of the Pyragas orbit in a semi-analytic way by inserting $\Lambda = i\Omega$ into Eq. (35) and separating the equation into real and imaginary parts:

$$
\begin{aligned}
\text{Real:} \quad 0 = {}& -\Omega^2 - 2\Omega b_0 \cos\beta \sin(\Omega\tau) \\
& -b_0(cr\sin\beta + a\cos\beta)\left[1 - \cos(\Omega\tau)\right] \\
& -b_0^2\, 2[1 - \cos(\Omega\tau)]\,\cos(\Omega\tau)
\end{aligned}
\tag{36}
$$

$$
\begin{aligned}
\text{Imag:} \quad 0 = {}& -a\Omega + 2\Omega b_0 \cos\beta\left[1 - \cos(\Omega\tau)\right] \\
& -b_0(cr\sin\beta + a\cos\beta)\,\sin(\Omega\tau) \\
& +b_0^2\, 2[1 - \cos(\Omega\tau)]\,\sin(\Omega\tau).
\end{aligned}
\tag{37}
$$

We can now use Ω as a parameter and solve the two equations for β and b_0 at each Ω. The resulting Hopf curve and the transcritical bifurcation curve (12) then form the boundary of the control domain (Fig. 11).

[1] E. Schöll and H. G. Schuster, eds., *Handbook of Chaos Control* (Wiley-VCH, Weinheim, 2008), second completely revised and enlarged ed.

[2] E. Ott, C. Grebogi, and J.A. Yorke, Phys. Rev. Lett. **64**, 1196 (1990).

[3] K. Pyragas, Phys. Lett. A **170**, 421 (1992).

[4] B. Fiedler, V. Flunkert, M. Georgi, P. Hövel, and E. Schöll, Phys. Rev. Lett. **98**, 114101 (2007).

[5] W. Just, B. Fiedler, M. Georgi, V. Flunkert, P. Hövel, and E. Schöll, Phys. Rev. E **76**, 026210 (2007).

[6] C. M. Postlethwaite and M. Silber, Phys. Rev. E **76**, 056214 (2007).

[7] S. Schikora, P. Hövel, H.-J. Wünsche, E. Schöll, and F. Henneberger, Phys. Rev. Lett. **97**, 213902 (2006).

[8] Y. Kuznetsov, *Elements of Applied Bifurcation Theory*, vol. 112 of *Applied Mathematical Sciences* (Springer-Verlag, 1995).

[9] B. Krauskopf and D. Lenstra, eds., *Fundamental Issues of Nonlinear Laser Dynamics*, vol. 548 (AIP Conference Proceedings, 2000).

[10] C. Bornholdt, J. Slovak, and B. Sartorius, Electron. Lett. **40**, 192 (2004).

[11] J. Slovak, C. Bornholdt, J. Kreissl, S. Bauer, M. Biletzke, M. Schlak, and B. Sartorius, IEEE Phot. Techn. Lett. **18**, 844 (2006).

[12] I. Kim, C. Kim, G. Li, P. LiKamWa, and J. Hong, IEEE Phot. Technol. Lett. **17**, 1295 (2005).

[13] M. Al-Mumin, C. Kim, I. Kim, N. Jaafar, and G. Li, Optics Communications **275**, 186 (2007).

[14] W. Lu and R. G. Harrison, Opt. Commun. **109**, 457 (1994).

[15] J. E. S. Socolar, D. W. Sukow, and D. J. Gauthier, Phys. Rev. E **50**, 3245 (1994).

[16] S. Yanchuk, K. R. Schneider, and L. Recke, Phys. Rev. E **69**, 056221 (2004).

[17] K. Engelborghs, T. Luzyanina, and G. Samaey, Tech. Rep. TW 330, Katholieke Universiteit Leuven (2001).

[18] V. Z. Tronciu, H. J. Wünsche, M. Wolfrum, and M. Radziunas, Phys. Rev. E **73**, 046205 (2006).

[19] E. Schöll and H. G. Schuster, eds., *Handbook of Chaos Control* (Wiley-VCH, Weinheim, 2008), chap. 21, second completely revised and enlarged ed.

[20] Note that due to the rotational symmetry of the system, the rotating waves $(a_1 e^{i\omega t}, n_1, a_2 e^{i\omega t}, n_2)$ are usually transformed into the family of equilibria $(a_1 e^{i\theta}, n_1, a_2 e^{i\theta}, n_2)$, $0 \leq \theta < 2\pi$ in the rotating coordinate system. For these equilibria, it is meaningful to speak about their eigenvalues. These eigenvalues coincide with the Floquet exponents of the original time-periodic rotating waves. An additional zero eigenvalue of these equilibria appears due to the symmetry.